

UCSF

UC San Francisco Electronic Theses and Dissertations

Title

Development of a Novel 2D RF Pulse Sequence to Achieve An Improved Localization of Hyperpolarized ^{13}C Imaging

Permalink

<https://escholarship.org/uc/item/7ch4z1cf>

Author

Tang, Shuyu

Publication Date

2013

Peer reviewed|Thesis/dissertation

**"Development of a Novel 2D RF Pulse Sequence to
Achieve An Improved Localization of
Hyperpolarized ^{13}C Imaging"**

by

Shuyu Tang

THESIS

Submitted in partial satisfaction of the requirements for the degree

of

MASTER OF SCIENCE in Biomedical Imaging

in the

GRADUATE DIVISION

of the

UNIVERSITY OF CALIFORNIA, SAN FRANCISCO

Copyright (2013)

By

Shuyu Tang

ACKNOWLEDGEMENT

I would like to acknowledge my advisor, Dr. Peder Larson, for offering me this great opportunity to get involved in this work while consistently teaching me and guiding me through the thesis process. I would like to thank other members of my thesis committee: Dr. Daniel Vigneron, Dr. David Saloner, and Dr. Duan Xu for generously donating their time and knowledge to this work. I am also grateful for all those who have provided the knowledge and assistance in the completion of this thesis work. Finally, I would like to thank the MSBI program and the UCSF department of Radiology for all resources and services that have been provided throughout the past year.

Development of a Novel 2D RF Pulse Sequence to Achieve An Improved Localization
of Hyperpolarized ^{13}C Imaging

By

Shuyu Tang

ABSTRACT

Hyperpolarization of metabolically active compounds labeled with ^{13}C has been recently utilized for imaging metabolic processes *in vivo*. This work focused on developing a new 2D radiofrequency (RF) pulse for tracking a ^{13}C -labeled pyruvate bolus injection *in vivo*. This pulse was designed for a clinical scanner, which allows for rapid translation to human studies. To meet clinical needs, we examined the flexibility of our design, and specifically the ability to shift the pulse location. The off-resonance response due to inhomogeneity, $[1-^{13}\text{C}]$ alanine and $[1-^{13}\text{C}]$ lactate have also been examined. Experimental results have validated the profile of our designed 2D RF pulse and off-resonance signals. To prepare for *in vivo* studies, our proposed pulse has been incorporated into a hyperpolarized ^{13}C imaging sequence.

TABLE OF CONTENTS

ACKNOWLEDGEMENT	iii
ABSTRACT	iv
LIST OF FIGURES	vi
INTRODUCTION	1
MATERIALS AND METHODS	2
RESULTS	8
DISCUSSION	12
CONCLUSION	14
REFERENCES	15

LIST OF FIGURES

Figure 1. <i>K</i> -space trajectory for a spiral 2D selective excitation.....	4
Figure 2. <i>K</i> -space trajectory, gradient waveform and slew rate waveform for constant-angular-rate spiral and constant-slew-rate spiral.....	6
Figure 3. A windowed jinc weighting function example.....	6
Figure 4. RF waveform that generates windowed jinc weighting on <i>k</i> -space.....	9
Figure 5. Surface plots of the selective volume.....	9
Figure 6. Simulation of the shifting property of the designed RF pulse.....	9
Figure 7. Off-resonance effects simulation.....	10
Figure 8. Mean and standard deviation signal collected inside and outside for the proposed 2DRF pulse within a range of off-resonance frequencies.....	10
Figure 9. Experimental demonstration of the excitation profile and off-resonance effects on the desired ROI.....	11
Figure 10. Surface plot of the ellipsoid selective volume.....	11
Figure 11. Off-resonance effects simulation at different pulse durations.....	12

INTRODUCTION

The term “hyperpolarization” refers to a procedure that redistributes ordinary nuclei energy level populations to significantly enhance polarization (1). With hyperpolarization, the signal from a given number of nuclear spins can be raised by a factor of 10,000 or more when compared with equilibrium conditions. This dramatic increase in signal has the potential to substantially overcome one of the key limitations of MR: limited sensitivity, allowing shorter scan times and to observe biomarkers with relatively low concentrations. Hyperpolarization of metabolically active compounds labeled with ^{13}C has been recently utilized for imaging metabolic processes *in vivo*. With the use of the chemical shift of the ^{13}C nuclei to distinguish between different molecular structures, separate images can be made of the injected compound as well as its metabolic products.

Selective excitation pulses are required to reduce sampling of the initially polarized substrate, thus leaving more polarization available for detection as newly subsequent metabolic products. Spatially 2D-selective radiofrequency (2DRF) excitation is an option due to its ability to excite arbitrarily shaped profiles within the plane defined by their trajectory. By reducing the excitation field-of-view (FOV), 2DRF pulses can also be used to improve the resolution or shorten the acquisition time. Previously, Vinding *et al* (2) designed an optimal-control 2D RF pulse to improve the localization for hyperpolarized ^{13}C imaging and tested the pulse on a phantom. In this work, we also designed a 2DRF pulse for localization improvement in hyperpolarized ^{13}C imaging but with major differences. First, the ultimate goal of

this new design is tracking ^{13}C -labeled pyruvate bolus in the selective volume *in vivo*, therefore, our 2DRF pulse was designed for a 3T clinical scanner with conventional gradient performances, which allows for translation to human studies. Second, to reduce the signal loss of hyperpolarized spins in bolus tracking, *k*-space analysis (3) for small-tip angles (STA) was used for our pulse design. In terms of acquisition methodology, Vinding *et al.* used a 180 degree refocusing slab pulse which could significantly reduce the hyperpolarized magnetization (4), and instead our approach uses echo-planar spectroscopic imaging (EPSI) readout (5) along the excited cylinder direction to localize to a specific slice location. The design of this 2DRF pulse has been completed and verified on a water phantom using a conventional proton-imaging sequence, and the pulse has been incorporated into a hyperpolarized ^{13}C imaging sequence with EPSI acquisition, ready for *in vivo* testing which is the next step of our study.

MATERIALS AND METHODS

Our 2D spatial-selective rf pulse was based on the *k*-space analysis (3) for small-tip angles. Iterative (6) and SLR (7) methods also can be used to design 2D RF pulses, but these methods are usually utilized for large-tip angles when the *k*-space method does not apply. The *k*-space method is described as follows.

Small-tip excitation solution as a *k*-space integral (3).

The Bloch equation in the rotating frame, neglecting T1 and T2, is

$$\frac{d}{dt} \begin{pmatrix} M_x \\ M_y \\ M_z \end{pmatrix} = \gamma \begin{pmatrix} 0 & G \cdot r & -B_{1,y} \\ -G \cdot r & 0 & -B_{1,x} \\ B_{1,y} & -B_{1,x} & 0 \end{pmatrix} \begin{pmatrix} M_x \\ M_y \\ M_z \end{pmatrix} \quad [1]$$

where M_x, M_y, M_z are magnetization in x, y, z axis, respectively, G is the amplitude of the linear gradient, $G = (G_x, G_y, G_z)$, B_1 is the amplitude of the applied RF field, γ is the gyromagnetic ratio and r is the position, $r = (x, y, z)$. Both G and B_1 are functions of time. We define the transverse magnetization as

$$M_{xy} = M_x + iM_y \quad [2]$$

and the applied RF field as

$$B_1 = B_{1,x} + iB_{1,y}. \quad [3]$$

Under the assumption of small tip-angle approximation, if the initial magnetization in the system is $(0, 0, M_0)$, Eq. [1] can be solved for transverse magnetization at time t ,

$$M_{xy}(\mathbf{r}, t) = iM_0 \int_{-\infty}^t \gamma B_1(\tau) e^{-i \int_{\tau}^t \gamma \mathbf{G}(s) \cdot \mathbf{r} ds} d\tau. \quad [4]$$

Defining a spatial frequency variable $\mathbf{k}(\tau, t)$ as

$$\mathbf{k}(\tau, t) = -\frac{\gamma}{2\pi} \int_{\tau}^t \mathbf{G}(s) ds \quad [5]$$

which is the integral of the remaining gradient waveform, then Eq. [4] may be rewritten

$$M_{xy}(\mathbf{r}, t) = iM_0 \int_{-\infty}^t \gamma B_1(\tau) e^{-i2\pi \mathbf{k}(\tau, t) \cdot \mathbf{r}} d\tau. \quad [6]$$

The transverse magnetization can also be expressed as a k -space integral, assuming the k -space trajectory does not cross itself.

$$M_{xy}(\mathbf{r}, t) = iM_0 \int_{\mathbf{k}} W(\mathbf{k}) S(\mathbf{k}) e^{-i\mathbf{k} \cdot \mathbf{r}} d\mathbf{k}. \quad [7]$$

where $W(\mathbf{k})$ is a spatial weighting function

$$W(\mathbf{k}(\tau, t)) = \frac{\gamma B_1(\tau)}{|\dot{\mathbf{k}}(\tau, t)|} \quad [8]$$

and $S(\mathbf{k})$ is a spatial frequency sampling function

$$S(\mathbf{k}) = \int_{-\infty}^t \delta(\mathbf{k}(\tau, t) - \mathbf{k}) |\dot{\mathbf{k}}(\tau, t)| d\tau, \quad [9]$$

which determines the area and the density of the k -space representation.

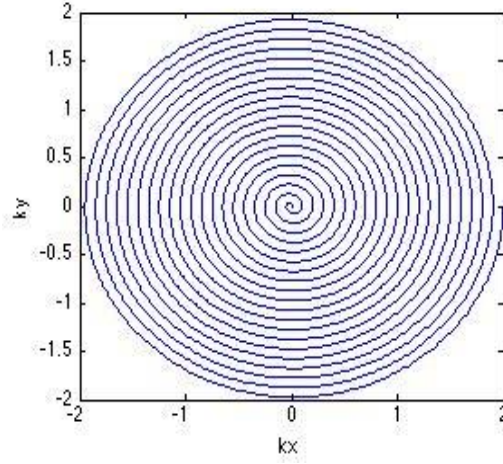


Figure 1. K -space trajectory for a spiral 2D selective excitation. The spiral starts at the outer edge and ends at the middle, so that the selected volume will be inherently refocused. This spiral has 20 cycles.

2D RF pulse design

The design starts by choosing a k -space trajectory. The k -space trajectory chosen for this project is a constant-slew-rate inward spiral (3)(10), which is a derivative of a constant-angular-rate inward spiral. A spiral trajectory is illustrated in Figure 1. “Inward” means that the spiral starts out at the edge, comes in and ends up at the origin of the k space. The “Inward” method holds the advantage of automatically refocusing the excited slice. We define the transverse k -space as

$$k_{xy} = k_x + ik_y \quad [10]$$

A constant-angular-rate inward spiral trajectory can be written as

$$\mathbf{k}_{xy}(t) = k_{max}\left(1 - \frac{t}{T}\right)e^{i2\pi N\left(1 - \frac{t}{T}\right)} \quad [11]$$

where the spiral has N cycles in a pulse duration T and k_{max} is the maximum radius of the spiral. N and k_{max} together determine the field of view. K -space, gradient and slew rate for a constant-angular-rate inward spiral trajectory are presented in

Figure 2a, where we observe that gradient and slew rate limits are reached only at the beginning of the waveforms, indicating an inefficient use of the gradient system. A constant-slew-rate spiral system, as shown in Figure 2b, can make the most of the gradient system and, thus, used in this project.

The next step is choosing a weighting function. Since the 2D RF pulse designed in this project aims to excite the ^{13}C -labeled pyruvate in a blood vessel, the desirable excitation profile is cylindrical. As shown in Figure 3, a Hamming-windowed jinc function is chosen as the weighting function, since the 2D Fourier Transform of a jinc function is a cylinder as desired and the windowing function is used to smooth the profile. The diameter and the resolution of the excited volume determine the weighting function. Using Eq. [8], the required RF waveform can be calculated as

$$B_1(\tau) = W(\mathbf{k}(\tau, t))|\dot{\mathbf{k}}(\tau, t)|/\gamma = W(\mathbf{k}(\tau, t))|\mathbf{G}(\tau)|. \quad [12]$$

In summary, for 2D spiral RF pulse design, field of view, resolution, gradient limit and slew limit are required to determine the k -space trajectory. The diameter of the excited cylinder and resolution are required to determine the weighting function. The desirable RF pulse waveform and gradient waveform can be calculated using k -space trajectory and the weighting function. Parameters of this project are: diameter 5mm, resolution 2.5mm, field of view 10cm, maximum gradient amplitude 4 G/cm, maximum slew rate 15 G/cm/ms, flip angle 5° . All the simulations were performed using MATLAB (The Mathworks Inc., Natick, MA). Experiments were performed on a General Electric EXCITE HDx 3T (Waukesha, WI) MRI system.

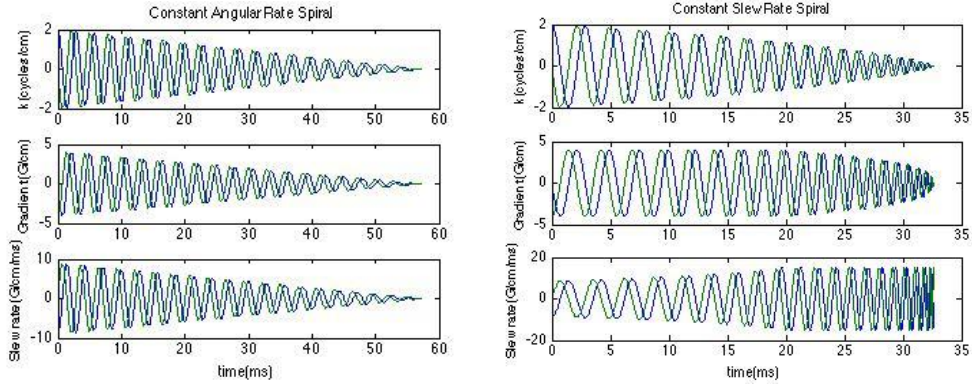


Figure 2. k -space trajectory, gradient waveform and slew rate waveform for (a) constant-angular-rate spiral and (b) constant-slew-rate spiral. Both of them will produce the k -space trajectory in Figure 1.

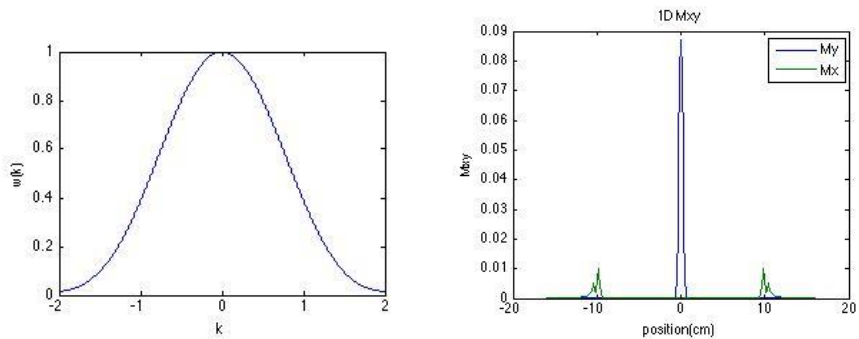


Figure 3. In a 1D view, a windowed sinc weighting function applied in k -space (left) excites the corresponding selective volume (right).

Other issues in 2D RF pulse design.

Voronoi Compensation (8). As indicated in Eq. [8] and Eq. [9], $|k'(\tau,t)|$ is an approximation of the density compensation function for $k(\tau,t)$. However, since the sampling direction in k space is not known, a higher gradient value doesn't necessarily indicate higher density. A better density compensation, the Voronoi algorithm, is used for this project. This algorithm divides the plane into small regions that are closest to each sample, and returns the area associated with each

sample. This area is the inverse of the density, therefore it is considered as density compensation function.

Ellipsoid shape. To make our design more flexible, the input k -space vector of weighting function in Eq. [12] has been modulated as Eq. [13] to achieve an ellipsoid surface for the excitation profile.

$$W_m(\mathbf{k}(\tau, t)) = W((\mathbf{k}_x(\tau, t)) * Dx/Dmax + (\mathbf{k}_y(\tau, t)) * Dy/Dmax) \quad [13]$$

,-Dx and Dy are the desirable diameters of the excitation profile in x and y directions, respectively, and Dmax is the larger diameter between Dx and Dy.

Shifting the volume. *In vivo* application necessitates the ability to shift the center location of the pulse. To shift the volume by r_o , the RF pulse needs to be modulated as

$$B_{1,m}(\tau) = B_1(\tau)e^{-i2\pi\mathbf{k}(\tau,t)\cdot\mathbf{r}_o}. \quad [14]$$

Off-resonance effects. In the excitation of a volume containing ^{13}C -labeled pyruvate, frequency shifts from alanine, lactate and main magnetic field inhomogeneity could result in excitation profile distortions. If the RF pulse is applied at an off-resonance frequency ω , it is equivalently modulated as

$$B_{1,m}(\tau) = B_1(\tau)e^{-i\omega\tau}. \quad [15]$$

The excitation profile at several selected off-resonance frequencies were investigated to ensure that our designed 2D RF pulse only excites pyruvate in the selected volume and is robust to some field inhomogeneity, while minimally perturbing the other metabolites.

Pulse sequence. To validate the excitation profile of simulation, a proton-imaging pulse sequence was developed using our 2D RF pulse and gradient waveforms, using a typical two-dimensional Fourier transform (2D-FT) readout. Experiments at on-resonance frequency and several off-resonance frequencies (inhomogeneity, alanine and lactate) were performed on a spherical water phantom. For *in vivo* applications, our designed RF pulse and gradient waveform were then built into a ^{13}C -imaging sequence with EPSI as the readout sequence. We expect the signal of lactate and alanine to be small, but even if they are not, EPSI still allows for specifically monitoring the pyruvate signal.

RESULTS

Figure 4-11 show the simulation and experimental results of this study. Figure 4 and Figure 5 present our designed RF waveform and corresponding magnetization profiles. Figure 6 demonstrates the ability to shift the pulse location. Figure 7-9 present the simulation of off-resonance signals at selective frequencies, corresponding experimental results as well as a quantitative analysis of off-resonance signals for a range of frequencies. Figure 10 demonstrates the simulation of an ellipsoid-shaped excitation profile. Figure 11 illustrates how excitation profiles change with pulse duration.

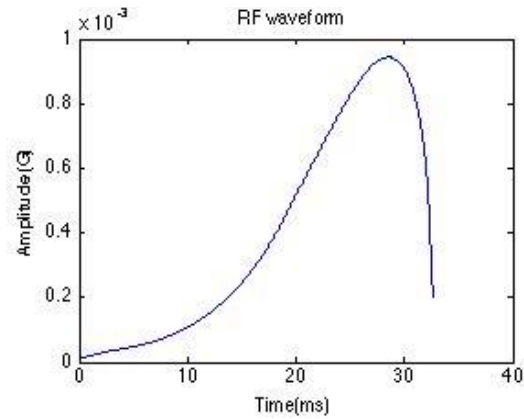


Figure 4. RF waveform that will produce a jinc function weighting of k -space when applied with the gradient waveforms shown in Figure 2b. The pulse is scaled to a tip angle of 5°

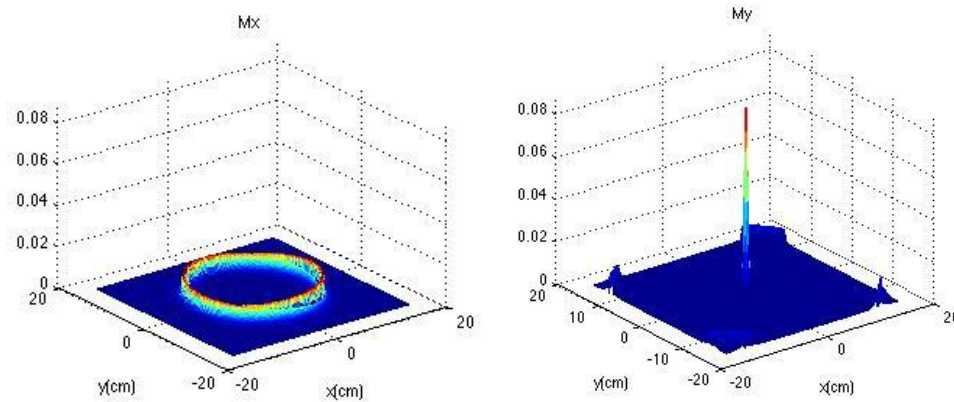


Figure 5. Surface plots of the selective volume produced by gradient waveform in Figure 2b and RF waveform in Figure 4. Note that all of the transverse magnetization is in M_y , meaning the selected volume is very well refocused. Sidelobes are very low.

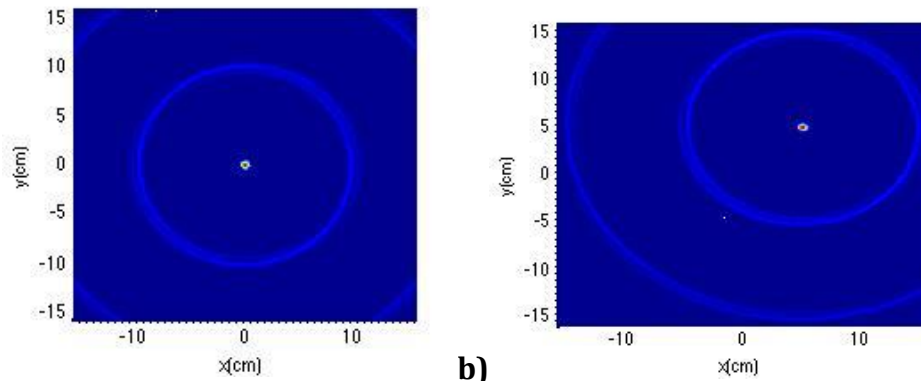


Figure 6. Shifting simulation: a): the selected volume same as Figure 5; b): the selected volume produced by modulated RF using Eq. [14], and the shifting vector is $(5, 5)$ cm.

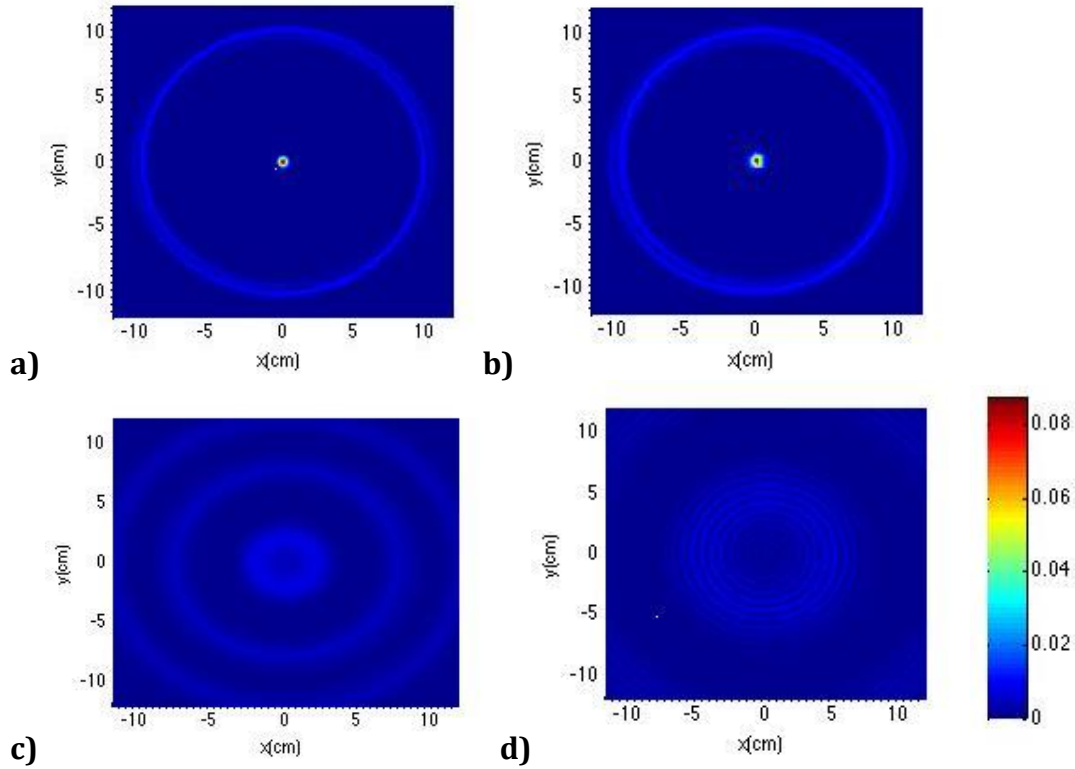


Figure 7. Off-resonance effects simulation. Graph a) is the selected volume produced using gradient waveforms in Figure 2a and weighting function in Figure 3. Graph b), c) and d) are produced by modulating the weighting function using 13 with off-resonance frequency (Hz) of 16 (0.5 ppm inhomogeneity at 3T), 176 (alanine) and 385 (lactate), respectively.

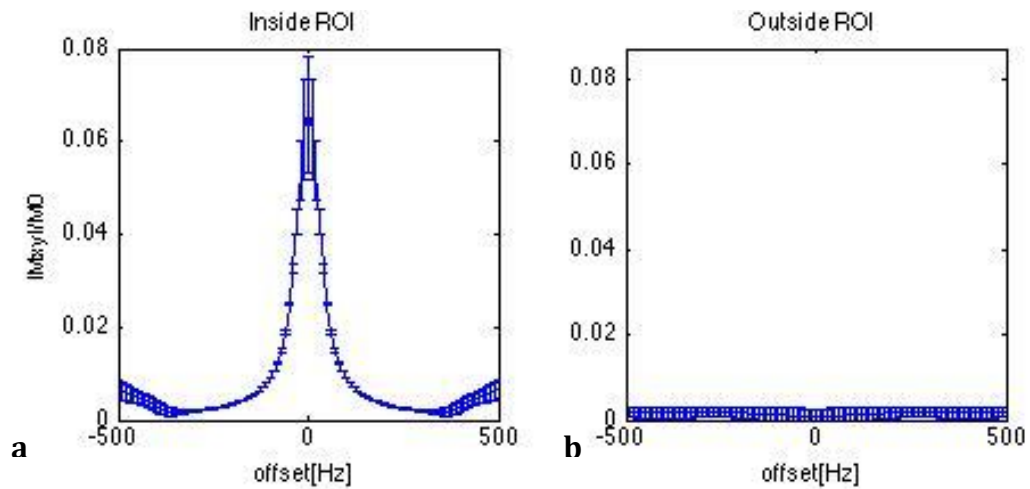


Figure 8. Mean and standard deviation signal collected inside (a) and outside (b) for the proposed 2DRF pulse within a range of off-resonance frequencies.

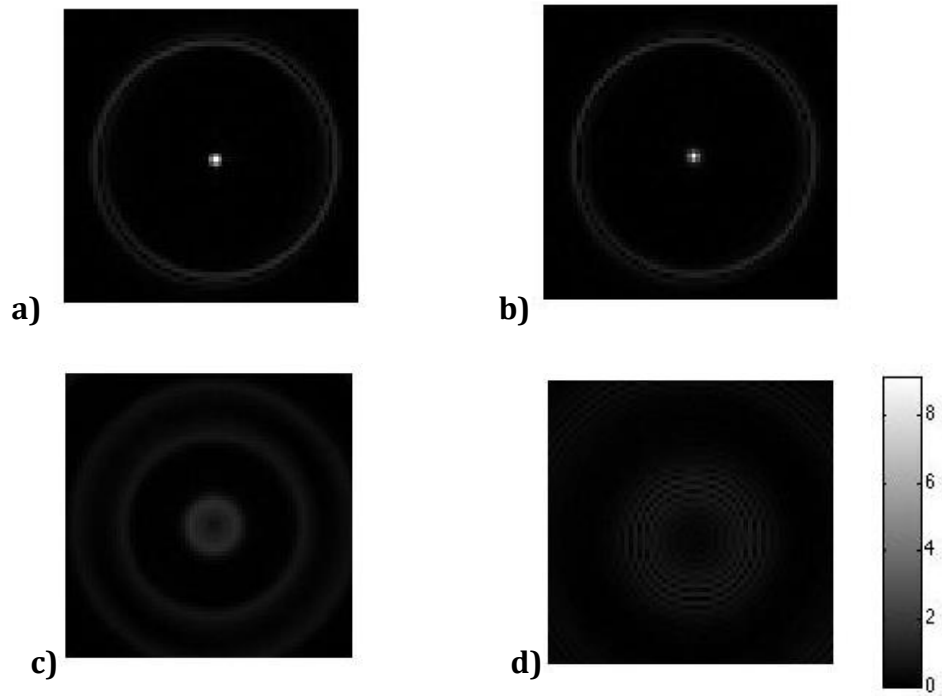


Figure 9. Experimental demonstration of the excitation profile and off-resonance effects on the desired ROI. Parameters used in each graph correspond to those in simulation (Figure 7).

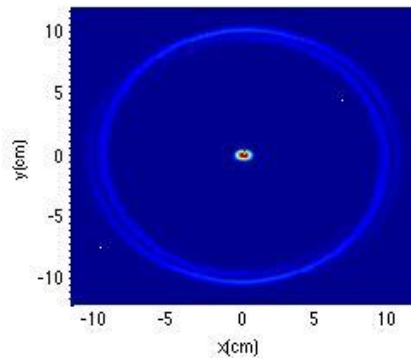


Figure 10. Surface plot of the ellipsoid selective volume. It was produced using modulated weighting function in Eq. [13]. The diameter in x and y direction is 1 cm and 0.5 cm, respectively.

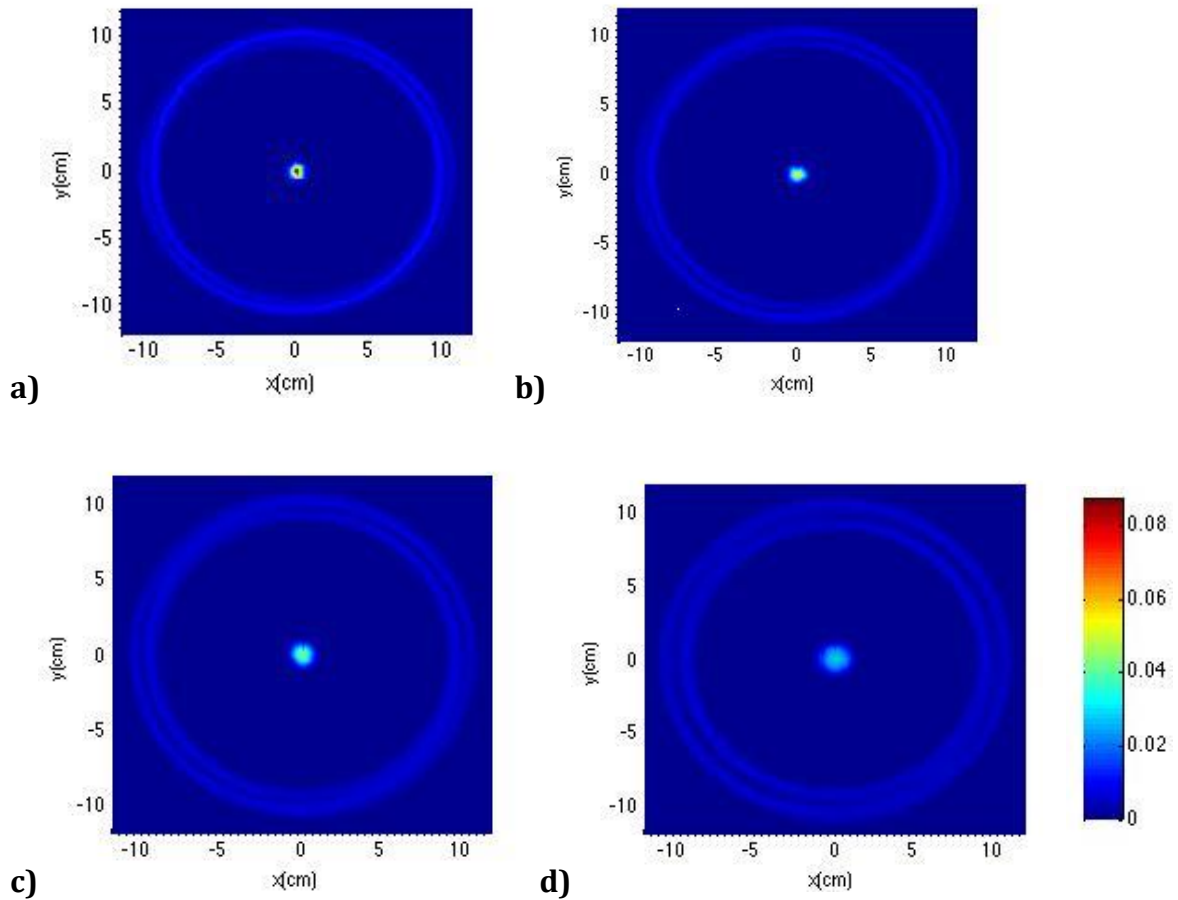


Figure 11. Off-resonance effects simulation at different pulse durations. Graph a) is the selected volume produced using gradient waveforms in Figure 2a and weighting function in Figure 4 with 16 Hz off-resonance. Graph b), c) and d) are produced by using pulse durations of 1.5, 2 and 3 times lengths, respectively, while keeping pulse shape and other parameters unchanged – As the pulse duration increases, the excitation profile becomes more sensitive to off-resonance.

DISCUSSION

The selective volume that results from the proposed gradient (Figure 2b) and RF pulse waveforms in Figure 4 is plotted in Figure 5. Note that there is theoretically no real component, meaning that the magnetization profile is well refocused. Figure 6 illustrates the ability to shift our RF pulse location, which enables moving the center of RF excitation to a specific location for *in vivo* applications.

By modulating the weighting function as shown in Eq. [13], we improved the flexibility of the selective volume of our proposed RF pulse. Figure 10 shows that our new RF pulse is able to excite an ellipsoid-shaped volume. To further enhance this design to achieve an arbitrarily-shaped excitation, two methods could be attempted in the future. Based on our current approach, we could use the Fourier transform of the desired shape as weighting function and interpolate it onto a k -space trajectory. The second method is to apply the optimal control approach proposed by Vinding et al. (2).

Spatial excitation profiles of different frequency offsets (inhomogeneity, lactate, alanine) are plotted in Figure 7. It was found that inhomogeneity does not cause dramatic change in the pattern and amplitude of the profile. In contrast, frequency offsets corresponding to alanine and lactate at 3T significantly distort and suppress the magnetization signal. Such findings are consistent with experimental results (Figure 9) and meet our expectation that our designed RF primarily excites pyruvate in ^{13}C imaging, while minimally perturbing other metabolites and being immune to ± 0.5 ppm magnetic field inhomogeneity at 3T. To estimate the frequency bandwidth of the pulse, we consider the total signal mean and standard deviation versus the offset of all the pixels inside and all the pixels outside the ROI, respectively (2). Figure 8 shows such profiles for the proposed pulse collected inside (a) and outside (b) the ROI. The profiles are calculated in the offset-range -1000 to 1000 Hz in increments of 10 Hz. The profile has a full-width half-maximum (FWHM) bandwidth

of approximately 80 Hz, which explains the magnetization profiles at our selected off-resonance frequencies for inhomogeneity, alanine and lactate.

A longer pulse duration will reduce the undesirable off-resonance signal but such a RF pulse will also be more sensitive to the main field inhomogeneity, as demonstrated in Figure 11. A larger FOV or higher resolution would result in a longer pulse duration and heighten the problem mentioned above. In reference to variable density compensation in reconstruction (9), variable density sampling in the excitation k -space could be utilized to keep the pulse duration unchanged while achieving a larger FOV or higher resolution.

CONCLUSION

We have designed a novel 2D RF pulse for tracking a ^{13}C -labeled pyruvate bolus *in vivo* while minimally perturbing the metabolic products of lactate and alanine. The parameters of our design are based on clinical scanner limits, which allows for translation to human studies. We have demonstrated the ability to shift the pulse center and the flexibility of our design. Off-resonance signals of inhomogeneity, alanine and lactate are desirable: inhomogeneity has little effects on the magnetization profile, while frequency offsets corresponding to alanine and lactate at 3T significantly distort and suppress the magnetization signal. Experimental results have verified the profile of our designed 2D RF pulse and its off-resonance response. To prepare for future *in vivo* studies, our new pulse has been incorporated into a hyperpolarized ^{13}C imaging sequence designed for human studies.

REFERENCES

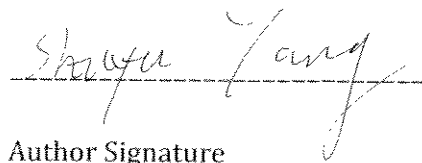
1. Kurhanewicz J, Vigneron DB, Brindle K, Chekmenev EY, Comment A, Cunningham CH, DeBeradinis RJ, Green GG, Leach MO, Rajan SS, Rizi RR, Ross BD, Warren WS, Malloy CR. Analysis of cancer metabolism by imaging hyperpolarized nuclei: prospects for translation to clinical research. *Neoplasia* 2011;13:81-97.
2. Vinding MS, Lasusten C, Maximov II, Sogaard LV, Larson JHA, Nielsen NC. Dynamic nuclear polarization and optical control spatial-selective ^{13}C MRI and MRS. *Journal of Magnetic Resonance* 2013;227:57-61.
3. Pauly J, Nishimura D, Macovski A. A k -space analysis of small-tip-angle excitation. *Journal of Magnetic Resonance* 1989;81:43-56.
4. Sonal J, Yen YF, Hurd R, Pfefferbaum A, Spielman D, Mayer D. Application of double spin echo spiral chemical shift imaging to rapid metabolic mapping of hyperpolarized $[1-^{13}\text{C}]$ -pyruvate. *Journal of Magnetic Resonance* 2011;209:332-336.
5. Mansfield P. Spatial mapping of the chemical shift in NMR. *Magnetic Resonance in Medicine* 1984;1:370-386.
6. Bottomley PA, Hardy CJ. Two -dimensional spatially selective spin inversion and spin-echo refocusing with a single nuclear magnetic resonance pulse. *Journal of Applied Physics* 1987;62:4284-4290.
7. Pauly J, Speilman D, Macovski A. Echo-planar spin echo and inversion pulses. *Magnetic Resonance in Medicine* 1993;29:776-782.
8. Aurenhammer F. Voronoi diagrams - a survey of a fundamental geometric data structure. *ACM Computing Surveys* 1991;23:345-405.
9. Pipe JG, Menon P. Sampling density compensation in MRI: rationale and an iterative numerical solution. *Magnetic Resonance in Medicine* 2000; 41:179-186.
10. Hardy CJ, Cline HE. Broadband nuclear magnetic resonance pulses with two-dimensional spatial selectivity 1989;66:1513-1516.

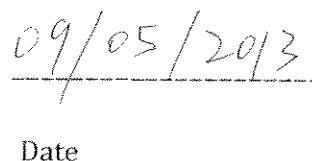
Publishing Agreement

It is the policy of the University to encourage the distribution of all theses, dissertations, and manuscripts copies of all UCSF theses, dissertations, and manuscripts will be routed to the library via the Graduate Division. The library will make all theses, dissertations, and manuscripts accessible to the public and will preserve these to the best of their ability, in perpetuity.

Please sign the following statement:

I hereby grant permission to the Graduate Division of the University of California, San Francisco to release copies of my thesis, dissertation, or manuscript to the Campus Library to provide access and preservation, in whole or in part, in perpetuity.


Author Signature


Date